Supporting Information

Ultrahigh Stable Methanol Oxidation Enabled by a High Hydroxyl Concentration on Pt clusters/MXene Interfaces

Jiexin Zhu[1,6], Lixue Xia[3,6], Ruohan Yu[1,6], Ruihu Lu,[2,3] Jiantao Li[1], Ruhan He[1], Yucai Wu[1], Wei Zhang[1], Xufeng Hong[1], Wei Chen,[1,5] Yan Zhao[3], Liang Zhou[1,4], Liqiang Mai[1,4,*], Ziyun Wang[2,*]

[1]State Key Laboratory of Advanced Technology for Materials Synthesis and Processing, Wuhan University of Technology, Wuhan 430070, Hubei, P. R. China.

[2]School of Chemical Sciences, The University of Auckland, Auckland, 1010, New Zealand

[3]International School of Materials Science and Engineering, Wuhan University of Technology, Wuhan 430070, Hubei, P. R. China.

[4]Foshan Xianhu Laboratory of the Advanced Energy Science and Technology Guangdong Laboratory, Xianhu hydrogen Valley, Foshan 528200, P.R. China.

[5]Hubei Key Laboratory of Ferro & Piezoelectric Materials and Devices, Hubei University, Wuhan 430062, Hubei, P. R. China.

[6]This authors contributed equally to this work.

*Email: ziyun.wang@auckland.ac.nz; mlq518@whut.edu.cn

Methods

Chemicals. Titanium aluminum carbide powders (>99 wt.%) were purchased from Laizhou Kai Kai Ceramic Mateirals Co. Ltd. Hydrogen fluoride (HF, 45%), Tetramethylammonium hydroxide solution (TMAH, 25% in water), Chloroplatinic acid hexahydrate ($H_2PtCl_6 \cdot 6H_2O$, AR), and potassium hydroxide (KOH, 99.999%) were purchased from Aladdin Industrial Inc. (Shanghai, China). Nafion solution (5 wt.%) was purchased from Alfa Aesar Chemical Co. Analytical grade methanol, ethanol, ethylene glycol, and glycerol were purchased from Sinopharm Chemical Reagent Co., Ltd. (Shanghai, China). Pt/C powders (20 wt.%, < 3.5 nm) were purchased from Shanghai Hesen Electric Co., Ltd. (Shanghai, China). All the chemicals were used without further purification.

Synthesis of $Ti_3C_2T_x$ MXene nanosheets. 2.0 g Ti_3AlC_2 powders were immersed into 30 ml 45% HF solutions in a clean polytetrafluoroethylene beaker and stirred for 24 h. The mixture was washed with deionized water until the pH of solution reached 6 ~ 7. Then, the black precipitates $Ti_3C_2T_x$ were transfer into 20 ml TMAH solutions and stirred for 10 days. The mixture was washed with deionized water three times at 10000 rpm to obtain intercalated $Ti_3C_2T_x$. The clay-liked precipitate was dispersed into 200 ml deionized water in three-necked flask and tip ultrasonicate for 2 h under ice bath with flow argon to prevent the oxidation of $Ti_3C_2T_x$. The suspension liquid was centrifuged for 30 min at 2500 rpm to remove the unstripped $Ti_3C_2T_x$ and collect the supernatant.

Synthesis of Ptc/$Ti_3C_2T_x$ and Pts/$Ti_3C_2T_x$. Ptc/$Ti_3C_2T_x$ electrocatalysts were prepared using spray drying technique. In a typical procedure, 1.0 ml of $H_2PtCl_6 \cdot 6H_2O$ solutions (9.65×10^{-2} M) and 100 ml $Ti_3C_2T_x$ nanosheets aqueous solutions were mixed uniformly and then delivered to spray dryer (Buchi B290). The Ptc/$Ti_3C_2T_x$ powders were collected and kept under dry conditions. The preparation process of Pts/$Ti_3C_2T_x$ was similar to that of Ptc/$Ti_3C_2T_x$ except that the dosage of $H_2PtCl_6 \cdot 6H_2O$ solutions were 0.1 ml.

Characterization. The morphology and elemental distribution of catalysts were performed by JEOL-7100F scanning electron microscope (SEM) and double spherical aberration corrected transmission electron microscope (Titan Cubed Themis G2 300/Titan Cubed Themis G2 30). The phase was determined by D8 Advance X-ray diffractometer using Cu-Kα radiation (λ = 1.5418 Å). XPS measurements were performed using AXIS SUPRA, Kratos. The XAFS spectrum of Pt L_3-edge were collected at room temperature in the fluorescence excitation mode at Beamline 12-BM-B at the Advanced Photon Source. The acquired XAFS raw data were background-subtracted, normalized, Fourier transformed, and integrated by standard procedures with the ATHENA program.

In-situ ATR-IR measurements. The in-situ ATR-IR spectrum was collected by a Thermo Scientific Nicolet iS50 FT-IR spectrometer equipped with MCT-A detector cooled by liquid nitrogen. The film working electrode was prepared by mixing 50 mg electrocatalysts and 5 μl PTFE solutions (40 wt%) and grinding into thin film. The film electrode was placed on the ZnSe prism and pressed by a Ti rod, and then assembled in a spectroelectrochemical cell with Pt wire as counter electrode and an Ag/AgCl electrode as reference electrode. All spectrum was obtained at a spectral resolution of 4 cm^{-1} and each single-beam spectrum was an average of 100 scans. A CHI 760e electrochemistry workstation (Shanghai CH Instruments, Inc.) was used for potential control.

Electrochemical measurements. The electrocatalyst powder inks were prepared using a mixture of 0.1 ml deionized water, 0.85 ml ethanol, 0.05 ml Nafion solution, 5 mg of the catalysts and 5 mg carbon black (Vulcan XC-72R) followed by ultrasonication for 30 min. Then, 10 μl of the ink was uniformly loaded onto a freshly polished glassy–carbon electrode (GCE, diameter = 0.5 cm), which was used as the working electrode yielding a catalyst loading of 0.25 mg cm^{-2}. All electrochemical measurements were performed by a conventional three-electrode system using an electrochemical workstation (CHI 760D, Shanghai CH Instruments, Inc.) and modulated speed rotator (MSR, AFMSRCE, rotate speed: 50-10000 rpm, PINE) in a 1 M KOH + 1 M CH_3OH solution. The GCE with electrocatalysts ink was used as the working electrode,

while platinum-black electrode and Hg/HgO were used as the counter electrode, and reference electrode. The rotate speed of MSR was keep at 1600 rpm. The MOR performances of electrocatalysts were recorded using CV scans from –0.9 V to 0.3 V vs. Hg/HgO at a scan rate of 10 mV s^{-1}. Durability test was performed by chronoamperometry at –0.1 V vs. Hg/HgO. The activity of ethanol, ethylene glycol, and glycerol oxidation reaction were performed in a 1 M KOH coupled with 1 M ethanol, ethylene glycol, and glycerol, respectively.

CO stripping test. For CO stripping test, the potential of the working electrode was maintained at –0.9 V vs. Hg/HgO while CO was bubbled into 1 M KOH solution for 30 min to form a monolayer CO on electrocatalysts. The dissolved CO was removed by bubbling the electrolytes with N_2 for 15 min. Stripping measurements were initiated from –0.9 V vs. Hg/HgO and first scanned in the anodic direction at 10 mV s^{-1} for at least two consecutive cycles.

DTF calculations. All spin-polarized DFT calculations on Ptc/$Ti_3C_2T_x$ were conducted by Vienna ab initio simulation package.[1] The projector-augmented wave (PAW) method and Perdew-Burke-Ernzerhof (PBE)[2-3] functional within the generalized gradient approximation (GGA) were applied to describe ionic cores and exchange-correlation effects, respectively. A cutoff energy of 450 eV was adopted and the Grimme method for DFT-D3 was used to account for van der Waals (vdW) interactions. The vacuum gap between periodic images was set to 15 Å to avoid the influence of periodic structure interactions. The convergence criteria for residual force and energy were set to 0.05 eV/Å and 10^{-5} eV, respectively. The Brillouin zone was sampled with a 2 × 2 × 1 Gamma centered special k points grid for geometry optimization. According to the computational hydrogen electrode (CHE) model proposed by Nørskov and co-workers,[4] the free energy of the proton-electron pair is equal to that of 1/2 H_2 (g). The free energy change for each fundamental step was determined by:

$$\triangle G = \triangle E + E_{ZPE} - T\triangle S$$

where $\triangle E$ is the difference of electronic energy directly obtained from DFT simulation. $\triangle E_{ZPE}$ is the contribution of variation of zero-point energy (ZPE), $\triangle S$ is the entropy (S) change, T is

the temperature (T = 298.15K) The ZPE and S of MOR intermediates were obtained by the vibrational frequencies. For the molecular in the gas phase, H_2 (g) and CO_2 (g), the ZPE and S were taken from NIST[5] database.

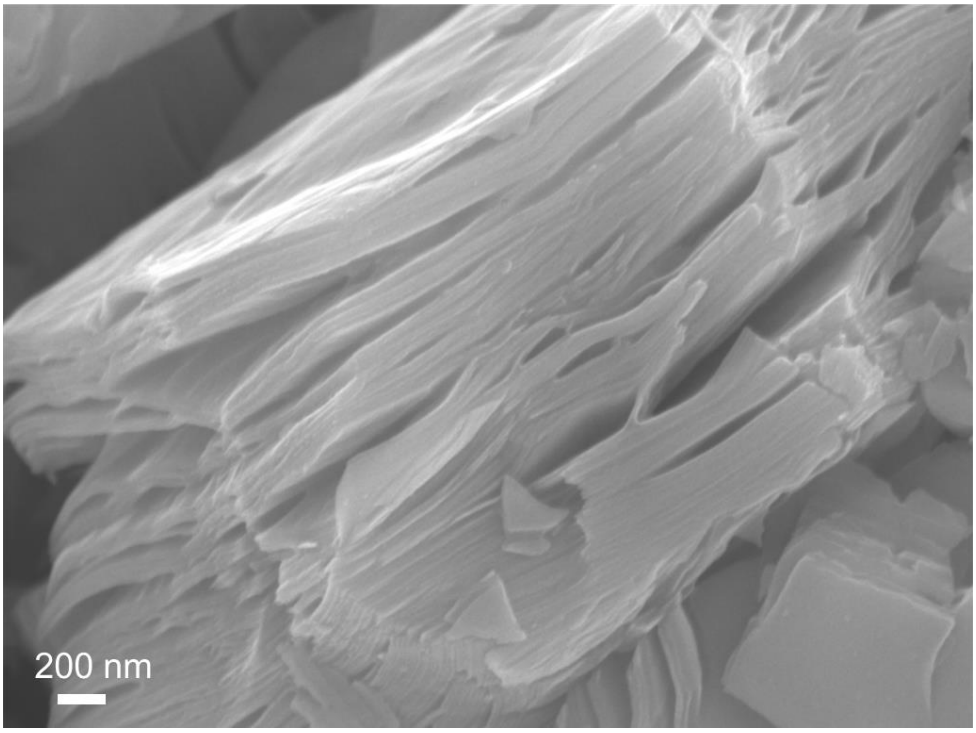

Figure S1. SEM image of accordion-like $Ti_3C_2T_x$ MXene.

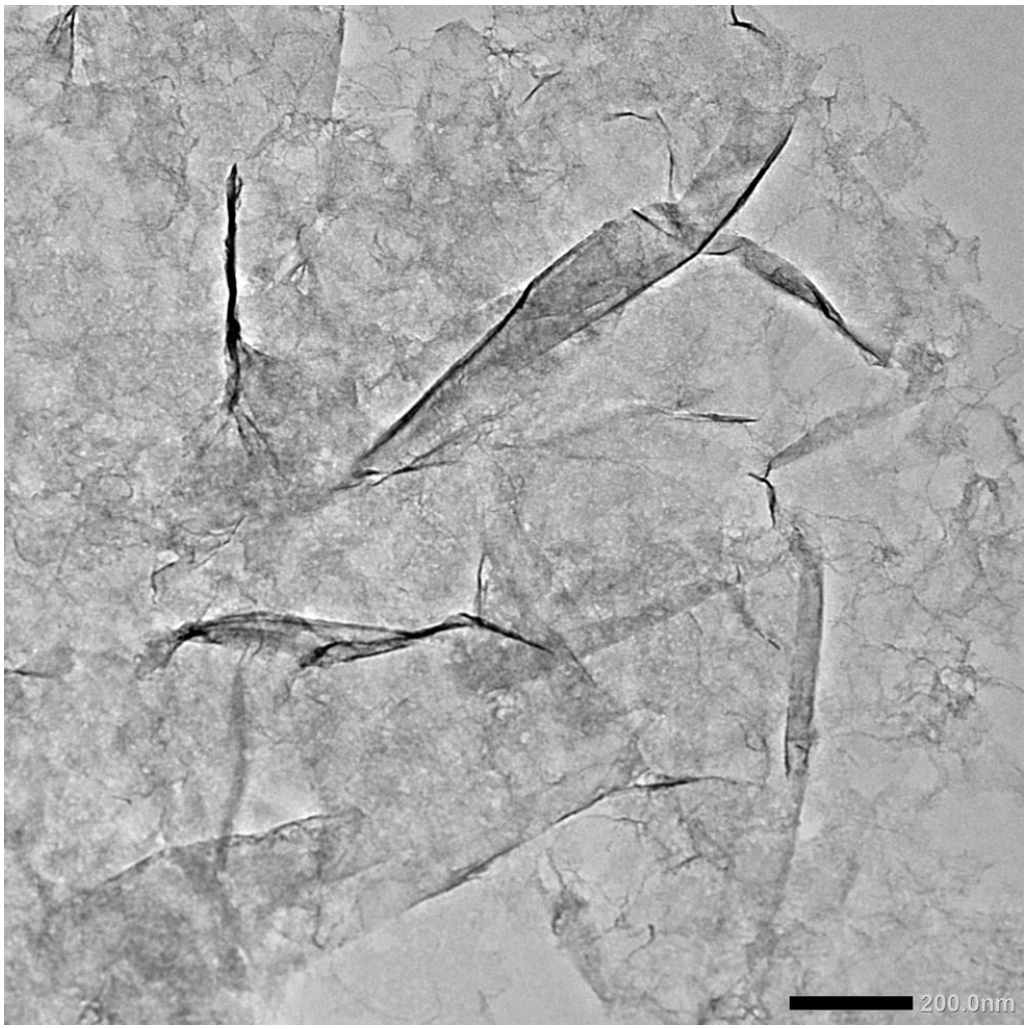

Figure S2. TEM image of $Ti_3C_2T_x$ nanosheets.

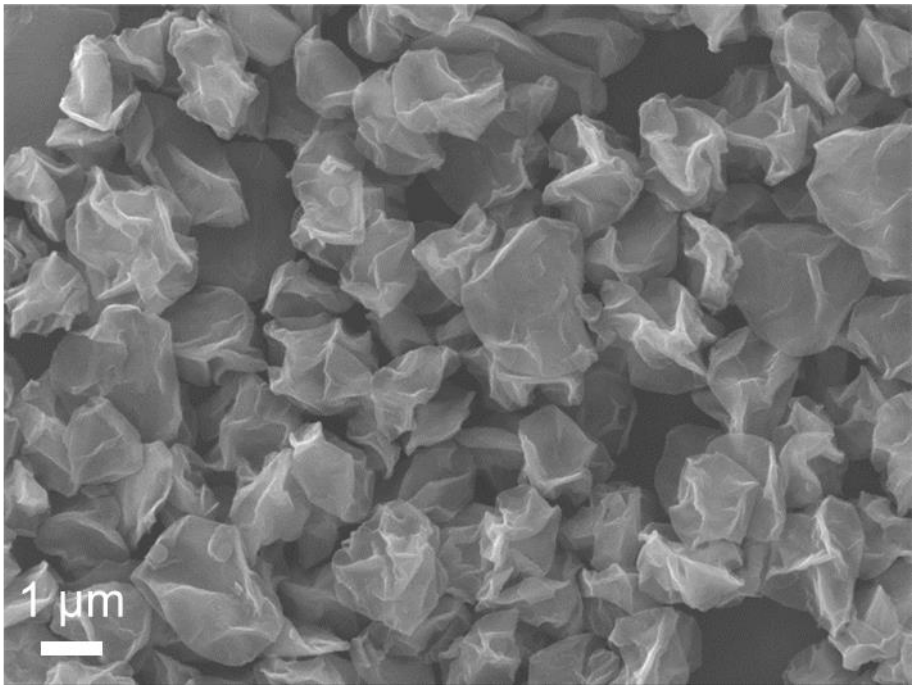

Figure S3. SEM image of Ptc/$Ti_3C_2T_x$.

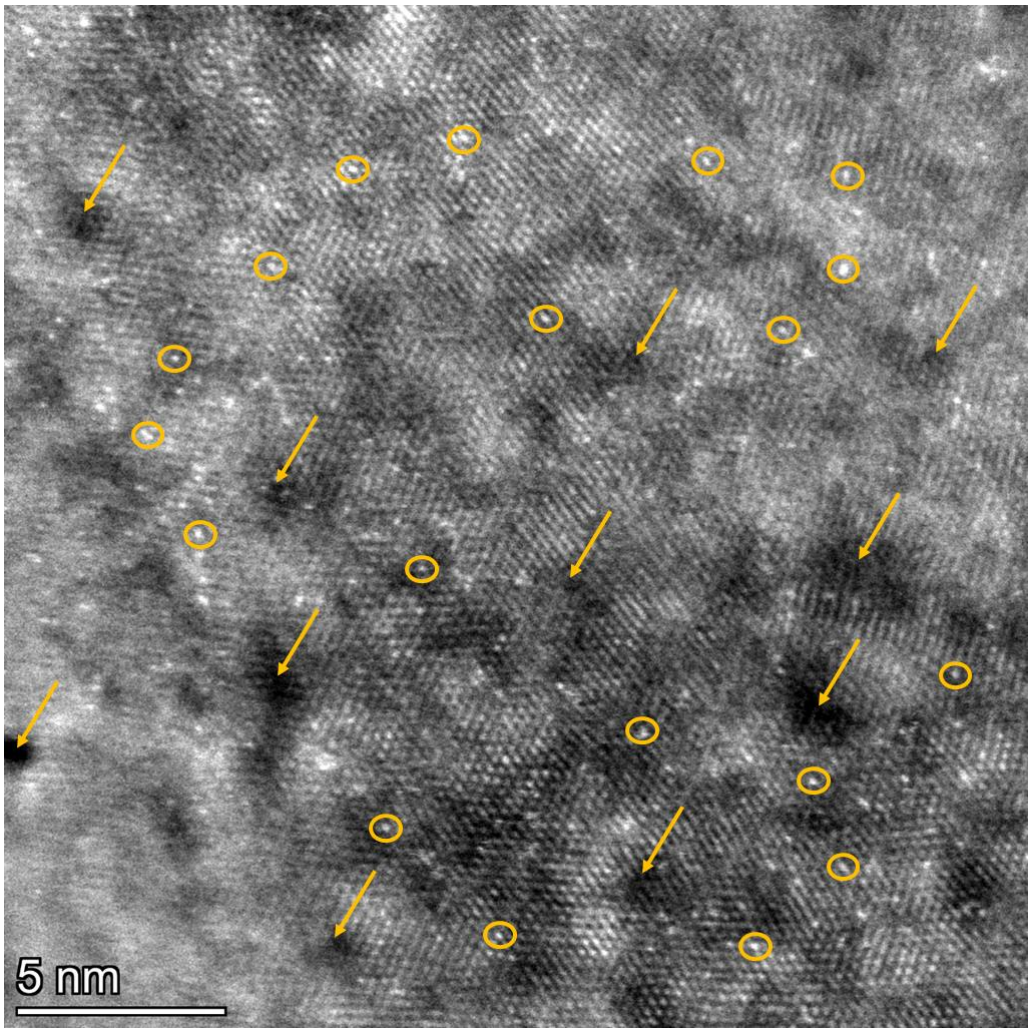

Figure S4. HAADF-STEM image of Pts/$Ti_3C_2T_x$. The bright dots marked by yellow circle represent the Pt single atoms, while.

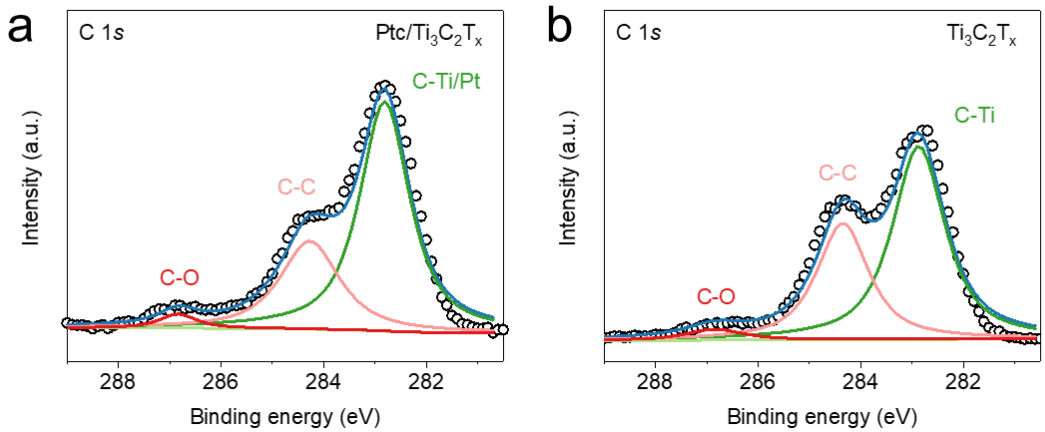

Figure S5. High-resolution XPS spectra for C 1*s* of Ptc/$Ti_3C_2T_x$ (**a**) and $Ti_3C_2T_x$ (**b**).

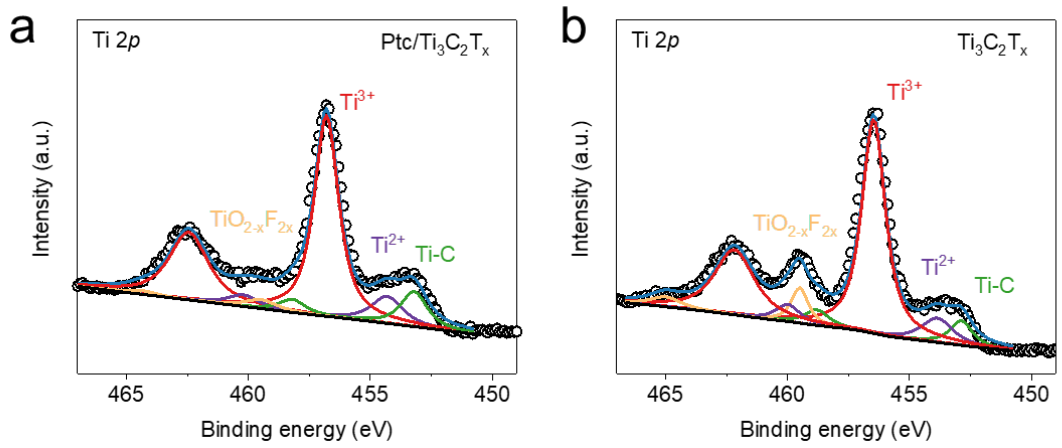

Figure S6. High-resolution XPS spectra for Ti 2*p* of Ptc/$Ti_3C_2T_x$ (**a**) and $Ti_3C_2T_x$ (**b**).

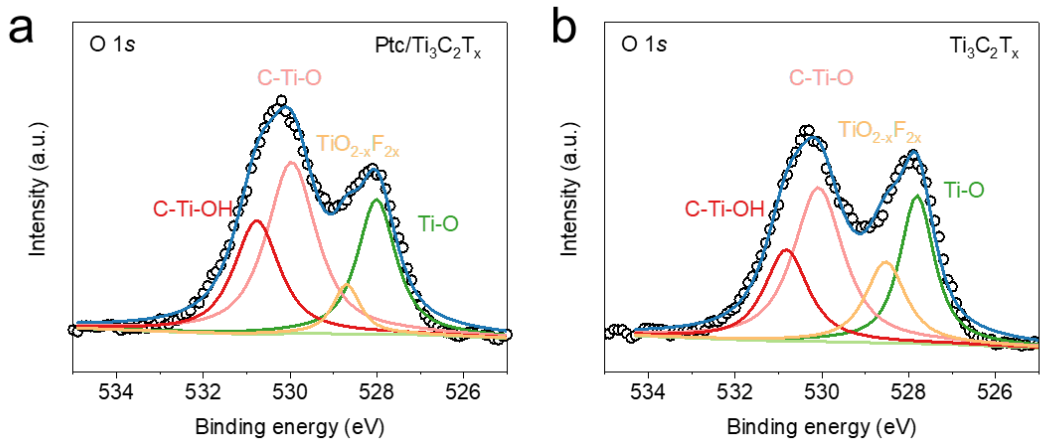

Figure S7. High-resolution XPS spectra for O 1*s* of Ptc/$Ti_3C_2T_x$ (**a**) and $Ti_3C_2T_x$ (**b**).

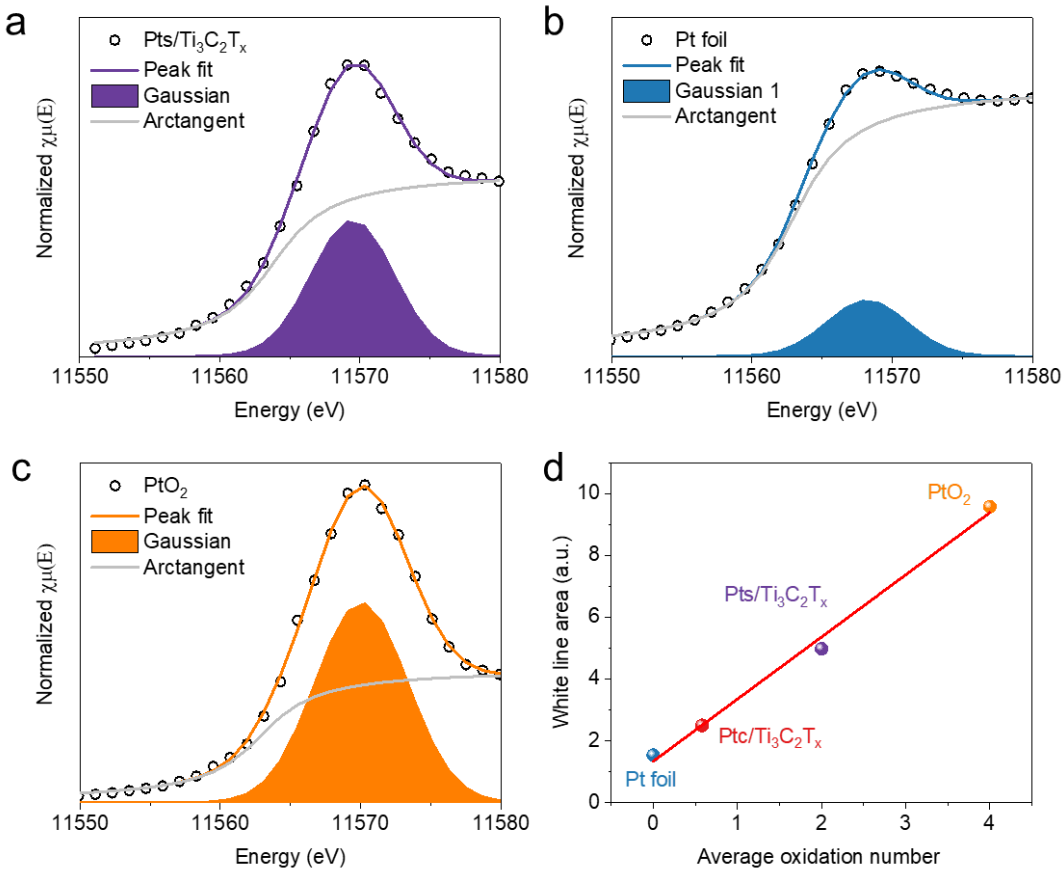

Figure S8. White line peak fitting analyses of Pt L_3-edge XANES spectra of (**a**) Pts/$Ti_3C_2T_x$, (**b**) Pt foil, and (**c**) PtO_2. (**d**) The fitted average oxidation number of Pt in Ptc/$Ti_3C_2T_x$ from XANES spectra.

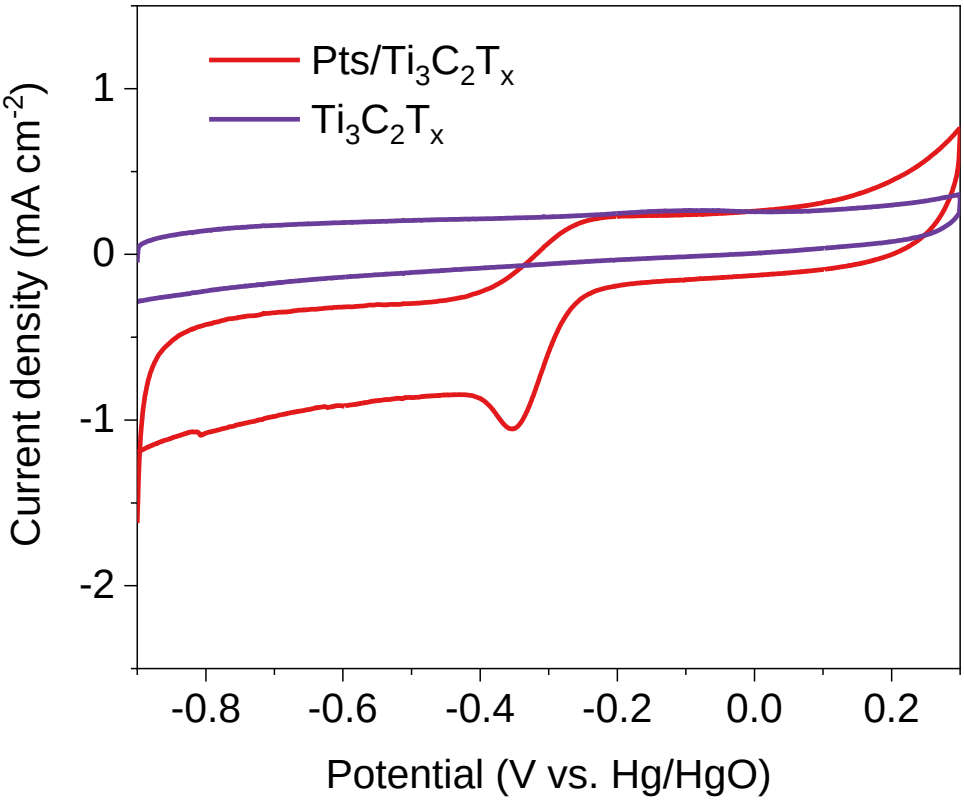

Figure S9. CV curves of $Pts/Ti_3C_2T_x$ and $Ti_3C_2T_x$ in 1 M methanol/1 M KOH.

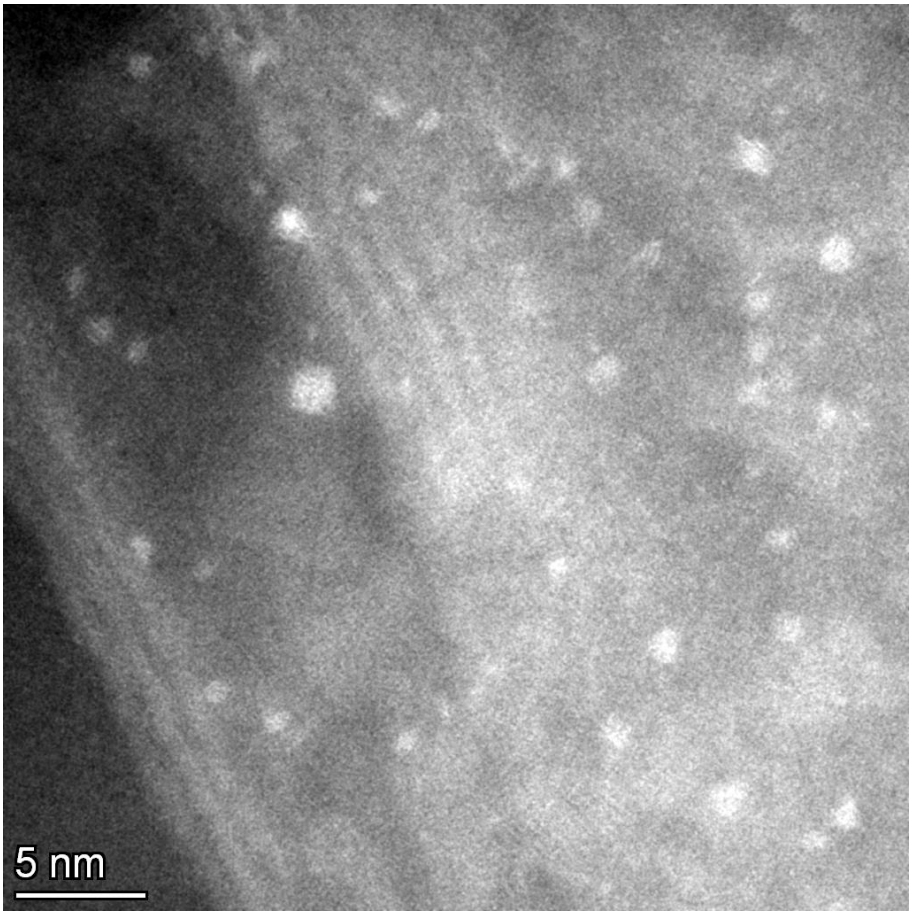

Figure S10. HAADF-STEM image of Ptc/$Ti_3C_2T_x$ after stability test.

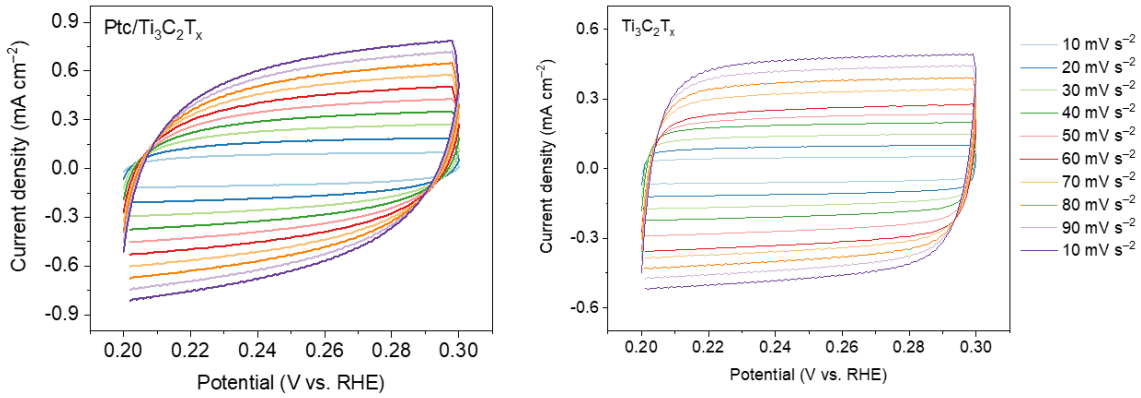

Figure S11. CV curves of $Ptc/Ti_3C_2T_x$ and $Ti_3C_2T_x$ at different scan rates.

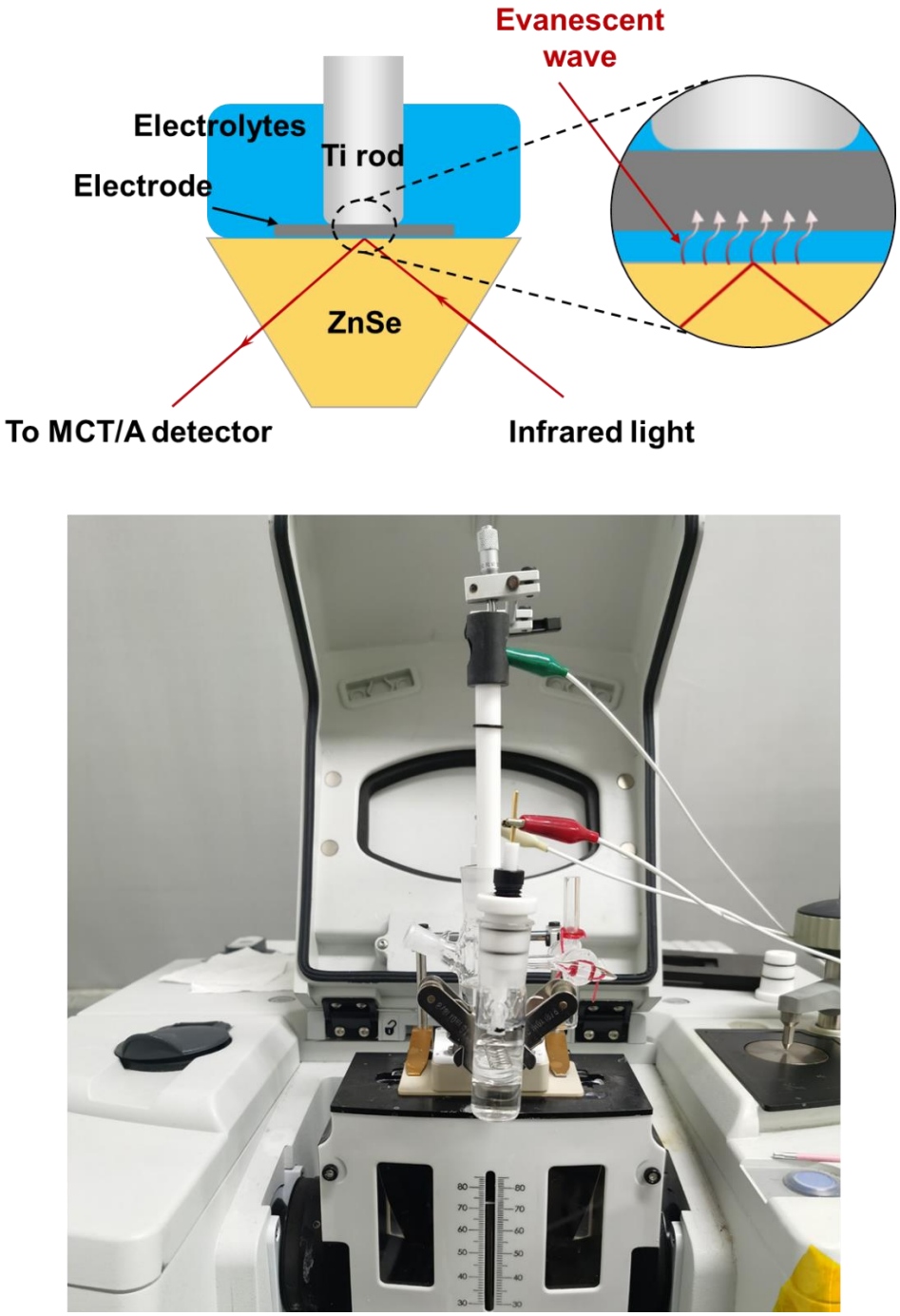

Figure S12. Schematic and optical photographs of in situ attenuated total reflection infrared (ATR-IR) test.

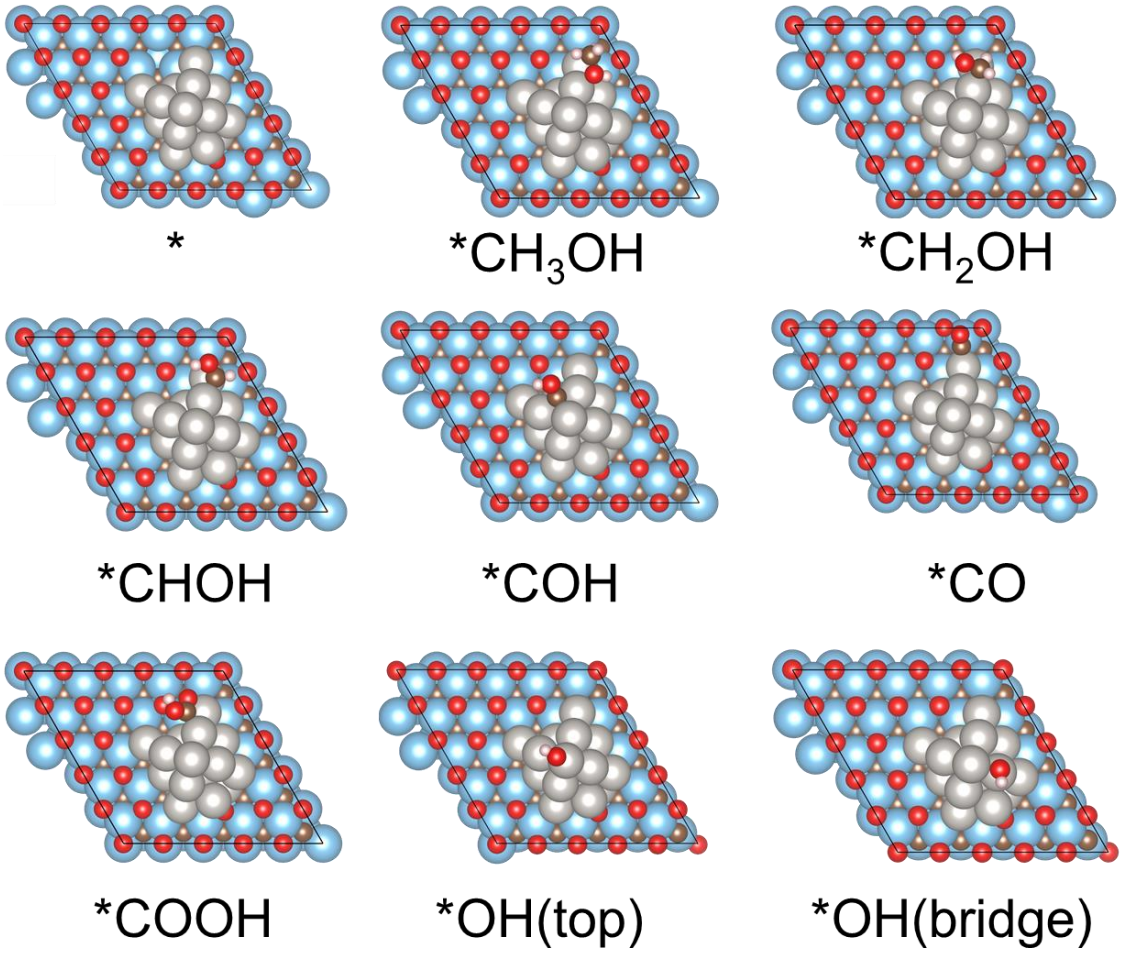

Figure S13. Ptc/$Ti_3C_2T_x$ (*) models and corresponding *CH_3OH, *CH_2OH, *CHOH, *COH, *CO, *COOH, and *OH adsorption.

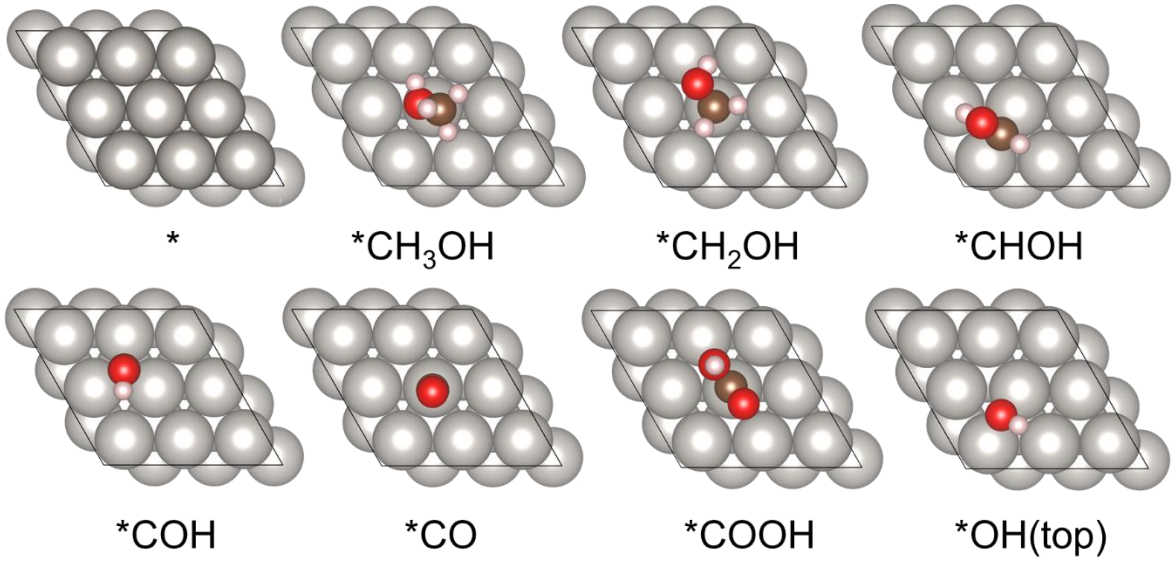

Figure S14. Pt (111) (*) models and corresponding *CH_3OH, *CH_2OH, *CHOH, *COH, *CO, *COOH, and *OH adsorption.

Table S1. Comparison of MOR performance of Ptc/$Ti_3C_2T_x$ with Pt-based electrocatalysts recently reported.

Catalysts	Electrolytes	Mass activity	durability	Reference
Ptc/$Ti_3C_2T_x$	**1 M KOH + 1 M CH_3OH**	**7.32A mg_{Pt}^{-1}**	**42% after 3000 min**	**This work**
Pt-skinned PtAg nanotubes	0.5 M H_2SO_4 + 0.5 M CH_3OH	0.738 A mg_{Pt}^{-1}	20.7% after 2000 s	[6]
1D PtFe alloy	0.1 M $HClO_4$ + 0.5 M CH_3OH	1.65 A mg_{Pt}^{-1}	88% after 10 000 cycles	[7]
PtRu alloy nanoparticles	0.1 M $HClO_4$ + 0.5 M CH_3OH	0.82 A mg_{Pt}^{-1}	63.67% after 800 cycles	[8]
AL-Pt/Pt_3Ga	0.5 M H_2SO_4 + 1 M CH_3OH	1.094 A mg_{Pt}^{-1}	20% after 1000 s	[9]
$BiO_x(OH)_y$-Pt	1 M KOH + 1 M CH_3OH	4.611 A mg_{Pt}^{-1}	33% after 10 000s	[10]
Pt NW/PDDA-$Ti_3C_2T_x$	0.5 M H_2SO_4 + 1 M CH_3OH	0.608 A mg_{Pt}^{-1}	20% after 2000 s	[11]
Pt/RGO−$Ti_3C_2T_x$	0.5 M H_2SO_4 + 0.5 M CH_3OH	1.102 A mg_{Pt}^{-1}	22% after 2000 s	[12]
PtRuNi FDs	0.1 M $HClO_4$ + 0.5 M CH_3OH	1.49 A mg_{Pt}^{-1}	78.5% after 1000 cycles	[13]
Pt/NbC	0.5 M KOH + 0.5 M CH_3OH	3.58 A mg_{Pt}^{-1}	95% after 100 cycles	[14]
PtAg alloy porous nanosheets	1 M KOH + 1 M CH_3OH	3.99 A mg_{Pt}^{-1}	27% after 2000 s	[15]
Pd_9Ru@Pt/FGN	0.5 M H_2SO_4 + 1 M CH_3OH	0.881 A mg_{Pt}^{-1}	85% after 500 cycles	[16]

References

[1] G. Kresse, J. Furthmüller, *Physical Review B* **1996,** *54*, 11169-11186.

[2] J. P. Perdew, K. Burke, M. Ernzerhof, *Phys. Rev. Lett.* **1996,** *77*, 3865.

[3] S. Grimme, *Journal of Computational Chemistry* **2006,** *27*, 1787-1799.

[4] J. K. Nørskov, J. Rossmeisl, A. Logadottir, L. Lindqvist, J. R. Kitchin, T. Bligaard, H. Jónsson, *The Journal of Physical Chemistry B* **2004,** *108*, 17886-17892.

[5] J. d. P. Peter Atkins, James Keeler, *Atkins' Physical Chemistry*. Oxford University Press: Oxford, U.K, 2017.

[6] Y. Ouyang, H. Cao, H. Wu, D. Wu, F. Wang, X. Fan, W. Yuan, M. He, L. Y. Zhang, C. M. Li, *Appl. Catal. B-Environ.* **2020,** *265*, 118606.

[7] L. Wang, X. L. Tian, Y. Xu, S. Zaman, K. Qi, H. Liu, B. Y. Xia, *J. Mater. Chem. A* **2019,** *7*, 13090-13095.

[8] L. Huang, X. Zhang, Q. Wang, Y. Han, Y. Fang, S. Dong, *J. Am. Chem. Soc.* **2018,** *140*, 1142-1147.

[9] Q. Feng, S. Zhao, D. He, S. Tian, L. Gu, X. Wen, C. Chen, Q. Peng, D. Wang, Y. Li, *J. Am. Chem. Soc.* **2018,** *140*, 2773-2776.

[10] X. Wang, M. Xie, F. Lyu, Y.-M. Yiu, Z. Wang, J. Chen, L.-Y. Chang, Y. Xia, Q. Zhong, M. Chu, *Nano Lett.* **2020,** *20*, 7751-7759.

[11] C. Yang, Q. Jiang, H. Huang, H. He, L. Yang, W. Li, *ACS Appl. Mater. Inter.* **2020,** *12*, 23822-23830.

[12] C. Yang, Q. Jiang, W. Li, H. He, L. Yang, Z. Lu, H. Huang, *Chem. Mater.* **2019,** *31*, 9277-9287.

[13] C. Shang, Y. Guo, E. Wang, *J. Mater. Chem. A* **2019,** *7*, 2547-2552.

[14] O. T. Ajenifujah, A. Nouralishahi, S. Carl, S. C. Eady, Z. Jiang, L. T. Thompson, *Chem. Eng. J.* **2021,** *406*, 126670.

[15] C. Shang, Y. Guo, E. Wang, *Nano Res.* **2018,** *11*, 6375-6383.

[16] C.-C. Kuo, S.-C. Chou, Y.-C. Chang, Y.-C. Hsieh, P.-W. Wu, W.-W. Wu, *J. Electrochem. Soc.* **2018,** *165*, H365.